Correlation between the conformational states of F_1-ATPase as determined from its crystal structure and single-molecule rotation

Daichi Okuno[a], Ryo Fujisawa[a], Ryota Iino[a], Yoko Hirono-Hara[b], Hiromi Imamura[a,c], and Hiroyuki Noji[a,1]

[a]The Institute of Scientific and Industrial Research, Osaka University, 8-1 Mihogaoka, Ibaraki, Osaka 567-0047, Japan; [b]Institute of Industrial Science, University of Tokyo, 4-6-1 Komaba, Tokyo 153-8505, Japan; and [c]Precursory Research for Embryonic Science and Technology, Japan Science and Technology Agency, 5 Sanbancho, Tokyo 102-0075, Japan

Edited by John E. Walker, Medical Research Council, Cambridge, United Kingdom, and approved November 6, 2008 (received for review June 18, 2008)

F_1-ATPase is a rotary molecular motor driven by ATP hydrolysis that rotates the γ-subunit against the $\alpha_3\beta_3$ ring. The crystal structures of F_1, which provide the structural basis for the catalysis mechanism, have shown essentially 1 stable conformational state. In contrast, single-molecule studies have revealed that F_1 has 2 stable conformational states: ATP-binding dwell state and catalytic dwell state. Although structural and single-molecule studies are crucial for the understanding of the molecular mechanism of F_1, it remains unclear as to which catalytic state the crystal structure represents. To address this issue, we introduced cysteine residues at βE391 and γR84 of F_1 from thermophilic *Bacillus* PS3. In the crystal structures of the mitochondrial F_1, the corresponding residues in the ADP-bound β (β_{DP}) and γ were in direct contact. The βE190D mutation was additionally introduced into the β to slow ATP hydrolysis. By incorporating a single copy of the mutant β-subunit, the chimera F_1, $\alpha_3\beta_2\beta$(E190D/E391C)γ(R84C), was prepared. In single-molecule rotation assay, chimera F_1 showed a catalytic dwell pause in every turn because of the slowed ATP hydrolysis of β(E190D/E391C). When the mutant β and γ were cross-linked through a disulfide bond between βE391C and γR84C, F_1 paused the rotation at the catalytic dwell angle of β(E190D/E391C), indicating that the crystal structure represents the catalytic dwell state and that β_{DP} is the catalytically active form. The former point was again confirmed in experiments where F_1 rotation was inhibited by adenosine-5′-(β,γ-imino)-triphosphate and/or azide, the most commonly used inhibitors for the crystallization of F_1.

ATP synthase | cross-link

The F_oF_1-ATP synthase is widely found in biological membranes such as the mitochondrial inner membrane, thylakoid membrane, and bacterial plasma membrane. It catalyzes ATP synthesis from ADP and inorganic phosphate (P_i) at the cost of the electrochemical potential of proton or sodium ion across the membrane (1–6). The synthase is composed of a water-soluble part, F_1, and a membrane-embedded part, F_o. F_1 is a rotary motor driven by ATP hydrolysis. The subunit composition of bacterial F_1 is $\alpha_3\beta_3\gamma\delta\epsilon$. The minimum complex of the rotary motor is the $\alpha_3\beta_3\gamma$ subcomplex that is hereinafter referred to as $F_1^{\alpha\beta\gamma}$. Hydrolyzing ATP, F_1 rotates the γ-subunit against the $\alpha_3\beta_3$ stator ring in a counterclockwise direction when viewed from the F_o (7). F_o is also a rotary motor that is driven by proton translocation across the membrane, down the electrochemical potential (8, 9). The subunit composition of bacterial F_o is ab_2c_{10-15} in which the c_{10-15} oligomer ring rotates against the ab_2 stator. These 2 rotary motors are connected through the central and peripheral stalks. Under ATP synthesis conditions where the proton electrochemical potential is dominant, F_o forcibly rotates the γ-subunit of F_1 in the reverse direction (clockwise when viewed from F_o). This reverse rotation of F_1 results in the reverse chemical reaction of ATP hydrolysis, i.e., ATP synthesis. Conversely, under ATP hydrolysis conditions, F_1 rotates γ in the anticlockwise direction with the c_{10-15} ring, forcing F_o to pump protons against the proton electrochemical potential.

The atomic-level structure of F_1 was first described in 1994, using a crystal of bovine mitochondrial F_1 (MF_1) prepared in the presence of ADP, adenosine-5′-(β,γ-imino)-triphosphate (AMP-PNP), and sodium azide (NaN_3) (10). This structure, referred to as the "reference structure," revealed that 3 α-subunits and 3 β-subunits are alternately aligned to form a hetero hexamer ring and the γ-subunit is set into the central cavity of the $\alpha_3\beta_3$ ring. The catalytic sites are located at each $\alpha\beta$ interface, mainly on the β-subunit. Each β is in a different conformational state depending on the bound substrate; one binds to AMP-PNP (β_{TP}), another to ADP (β_{DP}), and the third to none (β_{empty}). Both β_{TP} and β_{DP} are in the closed conformation where the C-terminal domain swings toward the nucleotide-binding domain to close the cleft between these domains. As a result, these β-subunits wrap the bound nucleotide tightly. In contrast, β_{empty} adopts an open conformation to weaken the affinity to the nucleotide. These structural features agree well with the binding change mechanism (5), which assumes that each catalytic site is in a different catalytic state and the interconversion of catalytic states drives the rotary motion of the γ-subunit, although there are some inconsistencies (11). Since this work, many crystal structures of MF_1 with different chemical inhibitors have been reported. The crystal structure that differs most from the reference structure is that which has ADP·AlF_4^-, where β_{empty} binds to ADP to adopt the half-closed conformation and the γ is twisted by $-20°$ (12). However, all other MF_1 structures have very similar conformations to the reference structure. Thus, the crystal structures of MF_1 essentially represent a certain stable conformational state of F_1 except for the ADP·AlF_4^--bound MF_1 structure.

In contrast, single-molecule studies on the γ rotation of F_1 have revealed that F_1 has 2 distinct stable conformations. Since the observation that F_1 performs a 120° step rotation of γ upon hydrolysis of 1 ATP, intensive attempts have been made to resolve the 120° step into multiple substeps to allow better understanding of how the elementary catalytic steps are coupled with the mechanical rotation. In many of these studies including this one, $F_1^{\alpha\beta\gamma}$ from thermophilic *Bacillus* PS3 (TF_1) have been used because TF_1 is stable under the harsh conditions of the single-molecule experiments and can be genetically modified. Thus far, 2 substeps have been found: the 80° and 40° substeps. High-speed imaging of the rotation (13) and a study of a mutant F_1 having a noticeably low ATP hydrolysis rate (14) revealed that the 80° substep is induced by ATP binding and that the 40° substep was initiated after hydrolysis

Author contributions: H.N. designed research; D.O., R.F., R.I., Y.H.-H., and H.I. performed research; D.O. and R.F. analyzed data; and D.O., R.I., and H.N. wrote the paper.

The authors declare no conflict of interest.

This article is a PNAS Direct Submission.

Freely available online through the PNAS open access option.

[1]To whom correspondence should be addressed. E-mail: hnoji@sanken.osaka-u.ac.jp .

This article contains supporting information online at www.pnas.org/cgi/content/full/0805828106/DCSupplemental.

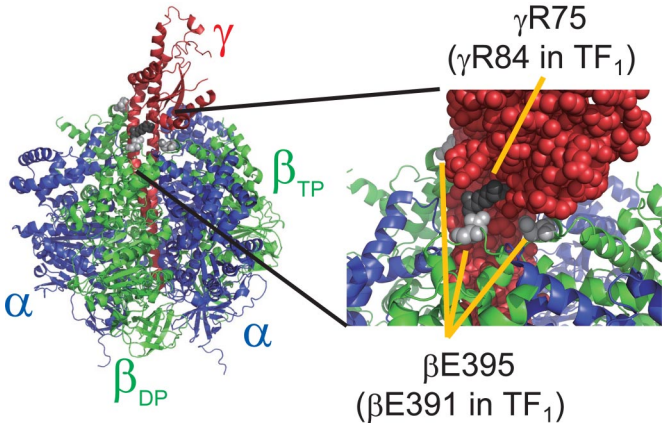

Fig. 1. Spatial positions of βE395 (light gray spheres) and γR75 (dark gray spheres) of MF_1 in the crystal structure (Protein Data Bank ID code 1e79) (26). These residues correspond to βE391 and γR84 of TF_1. The protruding part of the γ is the F_o binding side. The α-subunit is shown in blue, the β-subunit is green, and the γ-subunit is red. To show the βE395 and γR75 residues, R33, D74, D110, R113, R133, R134, and P135 residues of the γ were removed. The figure was produced with Pymol.

of bound ATP. Hereinafter, the 2 conformational states before the 80° or 40° substeps are referred to as the "binding dwell state" and "catalytic dwell state," respectively. Recent studies have suggested that ADP release and P_i release occur at the binding dwell angle and catalytic dwell angle, respectively (15, 16). More recently, a temperature-sensitive reaction was found at the binding dwell angle in a rotation assay at low temperature (16).

Thus, single-molecule studies have revealed that F_1 has 2 stable conformational states, whereas F_1 adopts essentially 1 specific stable conformation in the crystal structure. Which conformational state do the crystal structures of F_1 represent, binding dwell state, catalytic dwell state, or another new state? On this issue, there are some interesting results. The analysis of fluorescence resonance energy transfer (FRET) between fluorescent probes attached to β and γ suggests that the crystal structure probably corresponds to the catalytic dwell state (17). However, FRET measurement provides the relative distance between the fluorophores, but not the precise position in the 3D structure. Therefore, this result is not conclusive. The reference structure was recently revised to show that β_{DP} binds to N_3^- at the γ-phosphate binding position (18), implying that F_1 in the crystal structure is in the azide-stabilized form, while the feature of this structure was later revealed to be almost consistent with that of the catalytic ground state MF_1 (19). Taking into account that F_1 pauses at the catalytic angle when in the ADP-inhibited form (20), it seems plausible that the crystal structure is in the catalytic dwell state. However, there are no experimental results that clarify this point. In fact, a common view on the nature of crystal structure of the F_1 has not been established yet: some postulate it to be in the binding dwell state (21, 22) and others think it is the catalytic dwell state (23, 24).

Table 1. Distance between γ-carbons of βE395 and γR75 in crystal structures of MF_1

Protein Data Bank ID code	Ref.	Distance, Å		
		β_{TP}	β_{DP}	β_{empty}
1e79	26	11.2	6.1	25.1
1 h8e	12	11.1	6.0	17.8
1w0j	22	11.2	6.0	24.8
2ck3	18	10.8	5.7	ND
2jdi	19	11.0	5.8	ND
		11.0 ± 0.2*	5.9 ± 0.2*	22.6 ± 4.1*

ND, not determined because E395 in β_{empty} was not visible in these structures.
*Average ± SD.

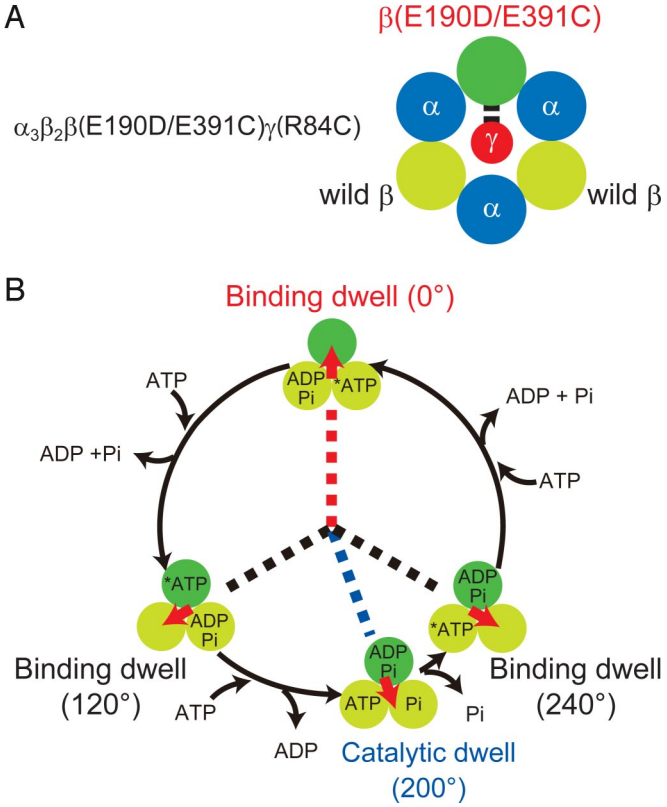

Fig. 2. The chimera $F_1^{\alpha\beta\gamma}$, $\alpha_3\beta_2\beta$(E190D/E391C)γ(R84C). (*A*) Schematic image of the chimera $F_1^{\alpha\beta\gamma}$, $\alpha_3\beta_2\beta$(E190D/E391C)γ(R84C) used in the cross-link experiment. Short black prongs denote cysteine residues at βE391 and γR84 for disulfide bond formation. (*B*) Circular diagram of the reaction and rotation of the chimera $F_1^{\alpha\beta\gamma}$. At 0°, the mutated β, β(E190D/E391C), binds ATP (red dotted line) and makes the long catalytic dwell at 200° (blue dotted line) casued by slowed ATP hydrolysis by the βE190D mutation (29). The wild-type β-subunits bind ATP at 120° or 240° (black dotted lines). The catalytic dwells by the wild-type β-subunits at 80° or 320° were too short (only 1 ms) to detect with the present recording system (33 ms per frame) and are not shown.

With an aim to addressing this issue, we generated a mutant $F_1^{\alpha\beta\gamma}$ from *Bacillus* PS3 in which cysteine residues were introduced at βE391 and γR84, respectively (25). In the crystal structures of bovine MF_1, corresponding residues in the ADP-bound β (β_{DP}) and the γ are in direct contact (18, 19, 22, 26). The residue of γR84 is a part of the "ionic track" (25, 27), which is the distinctive zonation of positively-charged residues around the axis of γ. It is postulated that β bends and unbends its conformation, tracing the ionic track with the negative charges of βD394 and βE395 (for MF_1) so as to convert the bending motion of β into the rotary motion of γ (27). The importance of the ionic track is supported by the analysis of mutant $F_1^{\alpha\beta\gamma}$ in which βE391 and γR84 are substituted with cysteine (25). Thus, the direct contact between βE391 and γR84 is the representative β_{DP}–γ interaction in the conformational state of the crystal structure. In this study, $F_1^{\alpha\beta\gamma}$ with βE391C and γR84C mutations was investigated in a single-molecule rotation assay to observe where it pauses when the introduced cysteine residues form a disulfide bond, thereby fixing the motor in the conformational state corresponding to the conformational state of the crystal structures. In addition to the cross-link experiment, the correlation between the crystal structures and the single-molecule experiment was studied by investigating at which angle $F_1^{\alpha\beta\gamma}$ stops rotation in the

BIOPHYSICS

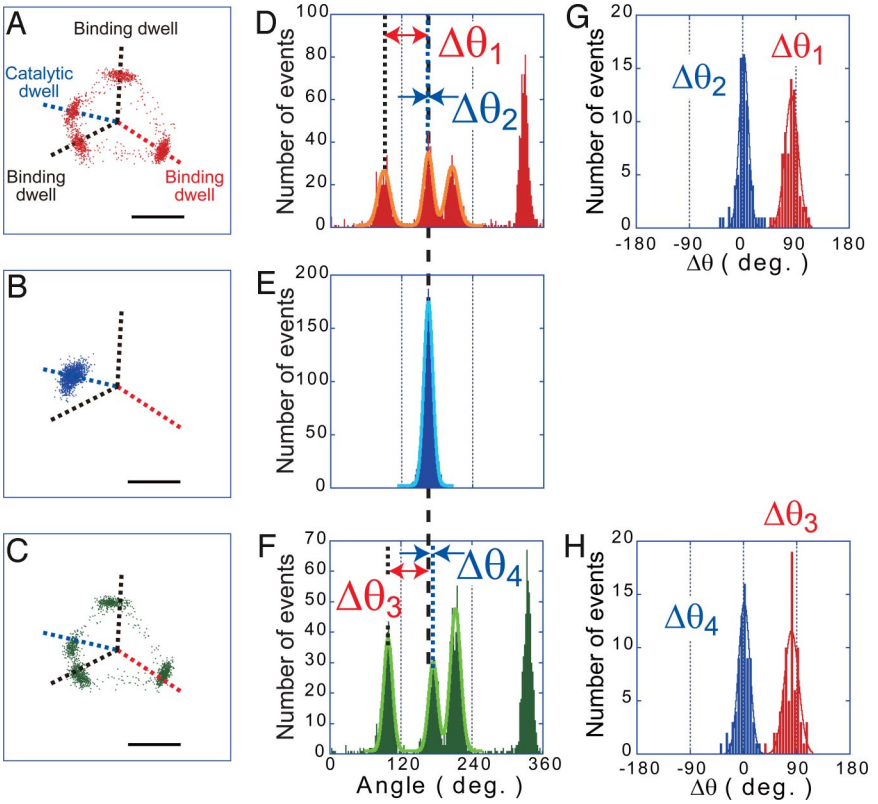

Fig. 3. β-γ cross-linking experiment in the single-molecule rotation assay. (*A–C*) The centroid traces of the rotation of a $\alpha_3\beta_2\beta$(E190D/E391C)γ(R84C) molecule. Data are derived from 60-s recordings. (*A*) The rotation at 200 nM ATP with 3 binding dwells by all β-subunits and 1 catalytic dwell caused by the β(E190D/E391C). (*B*) Pause of rotation after cross-linking by disulfide bond between βE391C and γR84C. (*C*) Rotation resumed after the reduction of the disulfide bond. (Scale bars: 100 nm.) (*D–F*) Histograms of rotary angle of traces shown in *A–C*. The angular positions of the pauses were determined by fitting the data with Gaussian curves (orange, light blue, and yellow green lines in *D*, *E*, and *F*, respectively). Then, the angular distance of the cross-link pause (dashed line in *E*) from the binding dwell angle on the clockwise side ($\Delta\theta_1$) or the catalytic dwell angle of βE391C ($\Delta\theta_2$) of the rotation before cross-link were determined. These distances were again determined by comparison with the rotation after reduction as $\Delta\theta_3$ and $\Delta\theta_4$. (*G* and *H*) Histograms of the angular distances ($\Delta\theta_1$ to $\Delta\theta_4$). $n = 72$ (36 molecules). The means $\pm$ SD for $\Delta\theta_1$, $\Delta\theta_2$, $\Delta\theta_3$, and $\Delta\theta_4$ were determined by Gaussian curve fitting (red and blue lines) to be 82.7 $\pm$ 15.9°, 2.0 $\pm$ 11.0°, 81.3 $\pm$ 17.0°, and 1.4 $\pm$ 13.5°, respectively.

presence of AMP-PNP and/or NaN_3, the most commonly used chemicals for the crystallization of F_1.

Results

A Chimera $F_1^{\alpha\beta\gamma}$, $\alpha_3\beta_2\beta$(E190D/E391C)γ(R84C). A mutant $F_1^{\alpha\beta\gamma}$ from *Bacillus* PS3 was prepared in which cysteine residues were introduced at βE391 and γR84, which correspond to the βE395 and γR75 of bovine MF_1, respectively. In the crystal structure of bovine MF_1, these 2 residues are in direct contact (Fig. 1). Although the whole structure of TF_1 has not been solved, it is most likely that TF_1 structure is very similar to MF_1, and that βE391 and γR84 of TF_1 are also in a very close proximity when TF_1 takes the conformational state corresponding to the crystal structure of MF_1. This is because F_1 from other species shows structural features essentially identical to that of MF_1 even if the amino acid sequence is not highly homologous to that of MF_1, as seen in the γ subunit of F_1 from *Escherichia coli* (EF_1): The structure of the γ of EF_1 is very similar to that of MF_1 (28), although the sequence homology against the γ of MF_1 is low (only $\approx$30%) the same as the γ of TF_1. Furthermore, the sequences around βE391 and γR84 are highly conserved in many species, suggesting the high structural conservation of these regions (Figs. S1 and S2). When βE391 and γR84 of $F_1^{\alpha\beta\gamma}$ from *Bacillus* PS3 were replaced with cysteine residues, they efficiently ($\approx$90%) formed a disulfide bond under oxidizing conditions within only a few minutes (25). Thus, it is reasonable to assume that TF_1 has the essentially identical structural features to MF_1. In the MF_1 crystal structure, the β that has direct contact with γR75 adopts the β_{DP} form. The γ-carbons of these residues that are in equivalent positions to the sulfur atoms of cysteine residue are only 5.9 Å away (Table 1), which is sufficiently close for disulfide bond formation. In contrast, the distances in the β_{TP}– or β_{empty}–γ pairs are 11 and 23 Å, respectively. Thus, the disulfide bond would be formed in the β_{DP}–γ pair. In the single-molecule rotation assay, γ was actually cross-linked to β only when the β was in a specific catalytic state, revealed to be the catalytic dwell state (see below). Furthermore, E190D mutation was introduced to the β-subunit in addition to E391C mutation. The mutant β(E190D/E391C)* was reconstituted with the wild-type β to build a chimera $F_1^{\alpha\beta\gamma}$, $\alpha_3\beta_2\beta$(E190D/E391C)γ(R84C), which has a single copy of β(E190D/E391C) (Fig. 2*A*). Here, the βE190D mutation was used as an angular position marker to determine the pause angle of cross-linked $F_1^{\alpha\beta\gamma}$. Shimabukuro *et al.* (14) showed that the βE190D mutation severely slows the hydrolysis step and causes the long pause (τ = 320 ms) at the catalytic angle. When a single copy of β with E190D mutation is incorporated in $F_1^{\alpha\beta\gamma}$, the reconstituted chimera $F_1^{\alpha\beta\gamma}$ exhibits a transient pause at the catalytic dwell angle of βE190D that is +200° from the angle at which the βE190D subunit binds to ATP (Fig. 2*B*) (29). Thus, a chimera $F_1^{\alpha\beta\gamma}$ with a single β(E190D) enables us to determine the pause angle of the cross-linked $F_1^{\alpha\beta\gamma}$ relative to the catalytic angle of β(E190D). It should be noted that a chimera $F_1^{\alpha\beta\gamma}$ with 1 β(E190D) was reported to exhibit another short pause at +120° from the catalytic dwell angle of β(E190D) (29). In this

*The designation subunit name (mutation name) indicates the subunit with the indicated mutations. The designation without parentheses indicates a mutation.

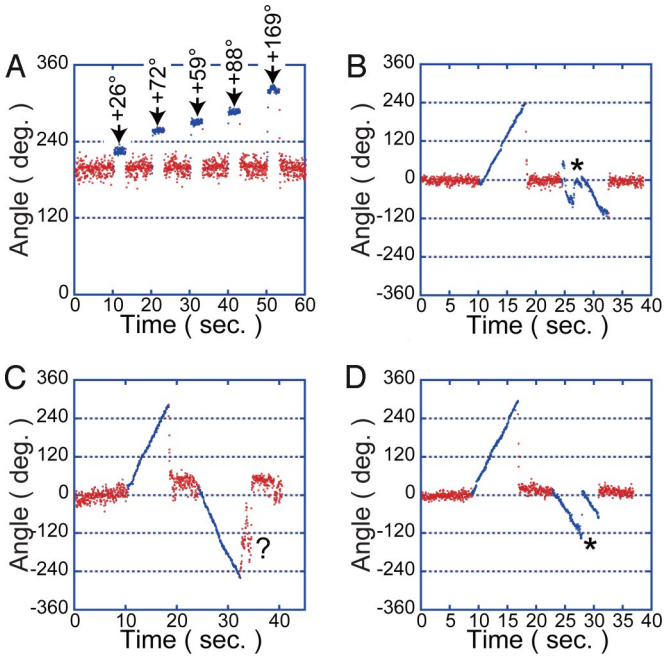

Fig. 4. Manipulation of cross-linked $F_1^{\alpha\beta\gamma}$ with the magnetic tweezers. (*A*) Time course of the manipulation. Blue dots represent the period for the manipulation. The molecule was clamped at the indicated angle for 3 s in the forward direction and released. (*B–D*) $F_1^{\alpha\beta\gamma}$ was rotated at the rate of 36° per s for near or >120° in both directions. When twisted in the backward direction, $F_1^{\alpha\beta\gamma}$ showed irregular responses. Some resisted the external magnetic field, inversed the magnetic moment of the beads instantaneously (at the point indicated by * in *B* and *D*), and then rotated back to the inversed angle of the original magnetic field (*B* and *D*), or some paused at irregular positions (indicated by a mark in *C*) after being released from the field.

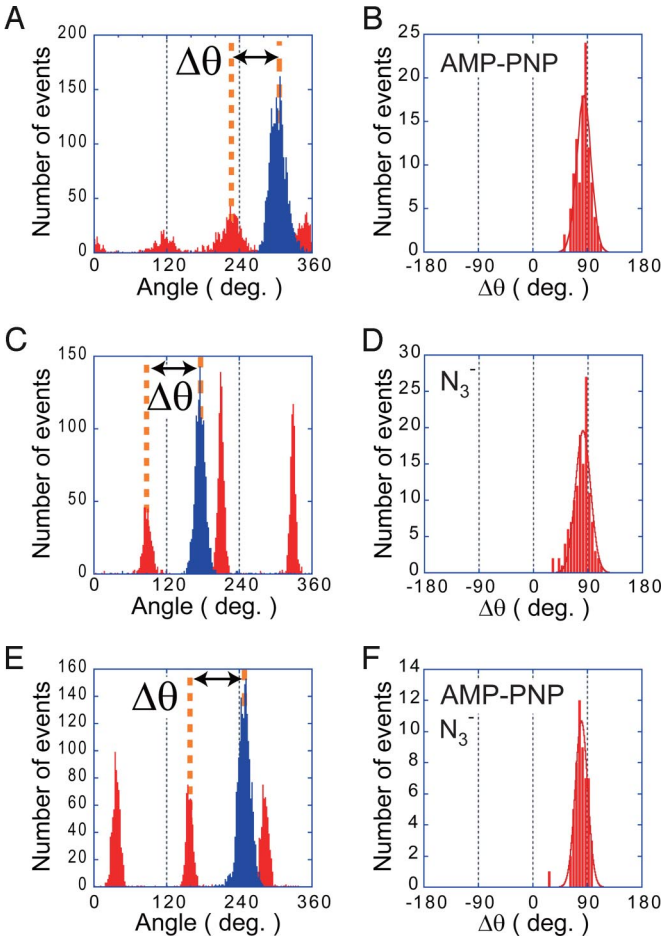

Fig. 5. Pausing position of $F_1^{\alpha\beta\gamma}$ stalled by chemical inhibitors. (*A*) Histogram of the angular position from a single experimental dataset of the AMP-PNP inhibition experiment. After observing active rotation of a molecule at 60 nM ATP, 1 μM AMP-PNP was infused into the reaction chamber with 60 nM ATP to stop the rotation. Red bars represent the angular position of free rotation; blue bars represent AMP-PNP inhibition. (*B*) Histogram of the angular deviation of the position of AMP-PNP inhibition from the binding dwell angle on the clockwise side ($\Delta\theta$ in *A*). The mean was 84.2 ± 16.3°. n = 107 (15 molecules). (*C* and *D*) The angular position of azide (N_3^-) inhibition. The rotation was inhibited by infusing 1 mM NaN_3 with 200 μM ATP. The mean value of $\Delta\theta$ was 81.9 ± 16.3°. n = 129 (29 molecules). (*E* and *F*) The angular position when inhibited by 200 μM AMP-PNP, 5 μM ADP, and 1 mM NaN_3. The mean value of $\Delta\theta$ was 80.2 ± 14.5°. n = 54 (9 molecules).

study, the short pause is neglected because the time constant of the short pause is too short ($\tau \approx 15$ ms) for the recording rate in this study (33 ms per frame).

Pausing Position of the Cross-Linked $F_1^{\alpha\beta\gamma}$. The rotation assay of $\alpha_3\beta_2\beta$(E190D/E391C)γ(R84C) was carried out under a substrate-limiting condition, at 200 nM ATP. Because the other kinds of chimera $F_1^{\alpha\beta\gamma}$, which carry 2, 3, or 0 of β(E190D/E391C) contaminated in the rotation assay, $\alpha_3\beta_2\beta$(E190D/E391C)γ(R84C) was identified based on 2 criteria. (*i*) The existence of obvious pauses in every turn at the 3 binding angles, 120° apart from each other. (*ii*) The existence of the clear pause in every turn at a catalytic angle, which divides 1 of 3 120° steps into the 80° and 40° substeps in this order (not 40° and 80° substeps) (Fig. 3*A* and *C*) (29). In the selection based on the first criterion, >95% of molecules were omitted from the further analysis because of ambiguous stepping. Among selected molecules, 50% showed the clear pausing at a catalytic angle and were identified as the chimera, $\alpha_3\beta_2\beta$(E190D/E391C)γ(R84C). The remaining were mostly $\alpha_3\beta_3\gamma$(R84C), of which all β-subunits were wild type, because the other chimera $F_1^{\alpha\beta\gamma}$ molecules carrying 2 or 3 mutant β-subunits were difficult to find out because of their slow rotary motion and the reconstitution efficiency of the mutant β was lower than that of the wild type as reported (29). Fig. 3 *A–F* shows a single dataset of the cross-link experiment. First, the free rotation of a $\alpha_3\beta_2\beta$(E190D/E391C)γ(R84C) molecule was observed to determine the angular position of the catalytic dwell of β(E190D/E391C) and the 3 binding dwell angles (Fig. 3 *A* and *D*). Then, an oxidizing buffer containing 3-carboxy-4-nitrophenyl disulfide (DTNB) was injected to the flow chamber to promote a disulfide bond formation between βE391C and γR84C. After the buffer exchange, which took several minutes, a significant fraction of the molecules (≈70%) stopped rotation (Fig. 3 *B* and *E*). The remaining would be molecules in which cysteine residue was modified with a biotin that blocks the disulfide bond formation. After observing a pause, a pausing $F_1^{\alpha\beta\gamma}$ molecule was manipulated with magnetic tweezers to confirm the β–γ cross-linkage (Fig. 4). Unlike ADP-inhibited $F_1^{\alpha\beta\gamma}$, cross-linked $F_1^{\alpha\beta\gamma}$ never resumes rotation, even when forcibly rotated more than +80°, which is sufficient to reactivate ADP-inhibited $F_1^{\alpha\beta\gamma}$ with nearly 100% efficiency (Fig. 4*A*) (30). Instead, cross-linked $F_1^{\alpha\beta\gamma}$ behaved as a twisted spring: when forcibly rotated and released, it just returned to the original pausing position. The angular velocity of return was always very fast (3.8 revolutions per s) and comparable with the ATP-driven rotation velocity at high ATP concentration (≈5 revolutions per s). In rare cases, $F_1^{\alpha\beta\gamma}$ exhibited irregular behaviors such as large fluctuations at an irregular position (Fig. 4 *B–D*). Such irregular behaviors were observed in some cases where cross-linked $F_1^{\alpha\beta\gamma}$ was rotated more than ±120° with the magnetic tweezers. This phenomenon is probably caused by the partial unfolding of the γ- or β-subunits. When the buffer was exchanged

BIOPHYSICS

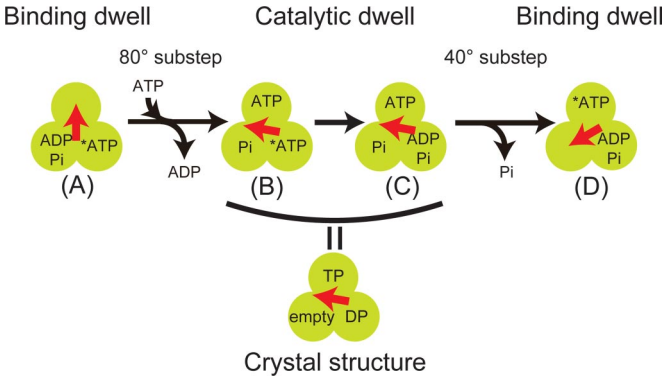

Fig. 6. The proposed reaction scheme of F_1 and correlation with the crystal structure. State A represents the binding dwell state. After ATP binding and ADP release, F_1 makes an 80° substep. Thereafter, F_1 hydrolyzes the tightly bound ATP (denoted by *) in the state transition from B to C. These states correspond to the crystal structure of F_1. After releasing P_i, F_1 makes a 40° substep to complete a cycle of ATP hydrolysis reaction coupled with 120° rotation. State D is the next binding dwell state.

with a reducing one, the disulfide bond was cleaved and $F_1^{\alpha\beta\gamma}$ molecules resumed active rotation (Fig. 3 *C* and *F*). Molecules that did not resume rotation or significantly changed their binding dwell angles were omitted from our data analysis. The angle differences of the cross-link angle (Fig. 3*E*) from the nearest binding angle on the clockwise side ($\Delta\theta_1$ in Fig. 3*D*) or the catalytic angle of β(E190D/E391C) ($\Delta\theta_2$ in Fig. 3*D*) were determined. These values were also determined by the comparison with the binding and catalytic dwell angles after reduction ($\Delta\theta_3$ and $\Delta\theta_4$ in Fig. 3*F*). For this analysis, the set of the experiments was repeated a total of 72 times with 36 molecules. The histograms of $\Delta\theta_1$ and $\Delta\theta_2$ showed a single peak and gave mean values of 82.7 ± 15.9° for $\Delta\theta_1$ and 2.0 ± 11.0° for $\Delta\theta_2$ (Fig. 3*G*). The histograms of $\Delta\theta_3$ and $\Delta\theta_4$ also gave essentially the same values, 81.3 ± 17.0° for $\Delta\theta_3$ and 1.4 ± 13.5° for $\Delta\theta_4$, showing the reproducibility of the experiment (Fig. 3*H*). These results show that the cross-linked $F_1^{\alpha\beta\gamma}$ pauses at the catalytic dwell angle of β(E190D/E391C). This means that the reference structure of MF_1 represents the conformational state of F_1 in the catalytic dwell state, and that β_{DP} conformation represents the catalytically active state that executes ATP hydrolysis. Considering that the standard deviations are much smaller than the magnitude of the 40° substep, cross-linked $F_1^{\alpha\beta\gamma}$ will not be stable at the binding angle.

Other chimera $F_1^{\alpha\beta\gamma}$ molecules, $\alpha_3\beta$(E190D)$_2\beta$(E391C)γ(R84C) and $\alpha_3\beta$(E190D)β(E391C)$_2\gamma$(R84C), were also examined to confirm that γR84C can form a disulfide bond with βE391C, which does not have the βE190D mutation. The rotation of $\alpha_3\beta$(E190D)$_2\beta$(E391C)γ(R84C) was rarely seen because of the low reconstitution efficiency of β(E190D) as described above. The cross-linked chimera paused at either of the 2 catalytic angles that did not correspond to the catalytic angle of βE190D (Fig. S3). Thus, it was verified that βE190D mutation does not affect the pause position of cross-linked $F_1^{\alpha\beta\gamma}$.

Pause Angle of $F_1^{\alpha\beta\gamma}$ Inhibited by AMP-PNP or N_3^-. To crystallize F_1, chemical inhibitors are often used to stabilize it in a specific conformational state. Another complementary method to correlate the crystal structure of F_1 and the substeps found in the single-molecule rotation assay is to analyze the pausing angle of $F_1^{\alpha\beta\gamma}$ inhibited by these inhibitors in the rotation assay. AMP-PNP and N_3^- are the chemical inhibitors most often used for the crystallization of F_1. Therefore, AMP-PNP and N_3^- were used to stop the rotation of $F_1^{\alpha\beta\gamma}$ in this experiment (Fig. 5). As in the cross-linking experiment, the 120° stepping rotation of a wild-type $F_1^{\alpha\beta\gamma}$ molecule was first observed under substrate-limiting conditions (60 nM ATP) to determine the 3 binding dwell angles. Then, the buffer containing an inhibitor (1 μM AMP-PNP or 1 mM NaN_3) was introduced into the flow chamber with 60 nM ATP for the AMP-PNP inhibition or 200 μM ATP for N_3^- inhibition. When the motor exhibited a long pause (>3 min), it was verified that the pause was not caused by ADP inhibition by forcibly rotating the motor through +80° with the magnetic tweezers; when inhibited by AMP-PNP or N_3^-, $F_1^{\alpha\beta\gamma}$ was never activated by this manipulation. However, when AMP-PNP- or N_3^--inhibited $F_1^{\alpha\beta\gamma}$ was forcibly rotated well over +80°, for example +180°, some molecules resumed rotation and stopped after a few turns. Such harsh manipulation would repel the tightly bound AMP-PNP- or N_3^--ADP from $F_1^{\alpha\beta\gamma}$. After determining the pause position of inhibited $F_1^{\alpha\beta\gamma}$, the buffer was replaced with the inhibitor-free ATP buffer to confirm the molecule was still active by observing the resumption of ATP-driven rotation. Fig. 5*A* shows the pause position under AMP–PNP inhibition. The red bars represent the angle distribution during the 120° stepping rotation, and blue bars represent the angle distribution when inhibited by the inhibitor mixture. The angular distance ($\Delta\theta$) of the AMP-PNP pause from the nearest binding angle on the clockwise side was determined (Fig. 5*B*) as in the above cross-link experiment. The mean angular distance was 84.2° ± 16.3°. This position corresponds to the catalytic dwell angle, consistent with the results of the cross-link experiment. The same result was obtained in the N_3^- inhibition experiments, and the mean angular distance of 81.9° ± 16.3° was obtained (Fig. 5 *C* and *D*). The pause angle of $F_1^{\alpha\beta\gamma}$ inhibited by 200 μM AMP-PNP, 5 μM ADP, and 1 mM NaN_3, which mimics the crystallization buffer of the reference structure, was also examined. The mean angular distance was 80.2° ± 14.5° (Fig. 5 *E* and *F*), essentially the same as the above experiments. Thus, many lines of experiments confirmed that the crystal structure of F_1 represents the catalytic dwell state found in the rotation assay.

Discussion

The crystal structure of F_1 was experimentally shown to represent the conformation of the catalytic dwell state found in single-molecule rotation assay. This means each β-subunit is in the β_{TP}, β_{DP}, or β_{empty} conformations during the catalytic dwell state. The β-γ cross-link using a chimera $F_1^{\alpha\beta\gamma}$ carrying 1 copy of β(E190D/E391C) showed that the catalytic angle of β(E190D/E391C) coincides with the pause position of $F_1^{\alpha\beta\gamma}$ where β_{DP} is cross-linked with γ. This finding means that the β_{DP} corresponds to the conformational state of the β that executes ATP hydrolysis reaction, consistent with theoretical works on quantum mechanics and molecular mechanics (31) or free-energy difference simulations (32). The crystal structure of BeF_3^--F_1, which is thought to mimic the catalytic intermediate state, also supports this result (22).

Fig. 6 shows the present reaction scheme of F_1, in which there are 2 chemical states during the catalytic dwell: prehydrolysis (state B) and posthydrolysis states (state C). Both states have the corresponding crystal structures. The recently reported structures (19, 33), the so-called "ground state" structures, in which both β_{TP} and β_{DP} bind with AMP-PNP correspond to the prehydrolysis state. However, the ADP·AlF_3-bound structure (34) would represent the posthydrolysis state. The azide-bound structures (10, 18) would also correspond to this state. Considering that β_{DP} represents the state that hydrolyzes ATP, β_{DP} corresponds to the β before and after executing hydrolysis (the β at the right bottom in states B and C). Consequently, β_{TP} conformation represents the ATP-bound state that was the ATP-waiting state in the prior binding dwell sate (state A in Fig. 6), and β_{empty} corresponds to the state after ADP release.

Thus, this study established the correlation between the conformational states of F_1 found in the crystal structures and the single-molecule rotation assay. However, there is one uncertain point in the reaction scheme, the timing of P_i release. The present model assumes that β_{empty} is the P_i-bound state, and after β_{empty} releases P_i, the 40° substep is triggered (state C to state D). This assumption is based on the recent study of the crystal structure of

yeast MF_1 (33) in which P_i binds to β_{empty}. The P_i-binding residues in the structure are consistent with those that biochemical studies have identified as the P_i binding site (35), supporting our reaction model. However, considering the other crystal structures that do not show an obvious electron density of P_i in the putative P_i-binding site, an alternative model is still possible; P_i is released from the β_{DP} immediately after hydrolysis. A clarification of this issue is the next challenging task in the study of the mechanochemical-coupling mechanism of F_1-ATPase.

Another issue is the structure of the binding dwell state. Although the ADP·AlF_4^--bound MF_1 shows obvious structural differences, the direction of the twist in the γ is opposite to our expectations. Therefore, ADP·AlF_4^--bound MF_1 is not in the binding dwell state. Rather, it might represent the intermediate state between state A and B of our reaction scheme in Fig. 6. Thus, there are no structural data about the binding dwell state. Because it is crucial for the understanding of the mechanochemical coupling mechanism of F_1, a crystallographic study of F_1 in the binding dwell state is one of the most important tasks for the understanding of the mechanism of F_1-ATPase. However, the fact that the crystal structures identified so far are comparable with the reference structure implies that the crystallization of F_1 in the binding dwell state is very difficult. One possible way is to crystallize F_1 at low temperature (16) or F_1 inhibited by tentoxin (36), where it spends most of the catalytic turnover time pausing at the binding dwell angle.

Materials and Methods

Preparation of $F_1^{\alpha\beta\gamma}$. Throughout this work, $\alpha_3\beta_3\gamma$ subcomplex of F_1-ATPase from thermophilic *Bacillus* PS3 (TF_1) was used. For inhibition by AMP-PNP or N_3^-, wild-type $F_1^{\alpha\beta\gamma}$ modified for the rotation assay α(His_6 at N terminus/C193S)$_3\beta$(His_{10} at N terminus)$_3\gamma$(S108C/I211C) was used. For simplicity, this $F_1^{\alpha\beta\gamma}$ was referred to as wild-type $F_1^{\alpha\beta\gamma}$ or $\alpha_3\beta_3\gamma$. For the β-γ cross-link experiment, cysteine residues were introduced into γR84 and/or βE391 of wild-type $F_1^{\alpha\beta\gamma}$ and $\alpha_3\beta$(E190D)$_3\gamma$ (14) to construct 4 mutants: $\alpha_3\beta_3\gamma$(R84C), $\alpha_3\beta$(E190D)$_3\gamma$(R84C), $\alpha_3\beta$(E391C)$_3\gamma$(R84C), and $\alpha_3\beta$(E190D/E391C)$_3\gamma$(R84C). Mutagenesis to construct the expression vectors of these mutants was performed as per the previous report on β-γ cross-linking (25). The mutants of $F_1^{\alpha\beta\gamma}$ were expressed in *E. coli*, purified, and biotinylated as reported (37). For the reconstitution of the chimera, $\alpha_3\beta_2\beta$(E190D/E391C)γ(R84C), solutions of $\alpha_3\beta_3\gamma$(R84C) and $\alpha_3\beta$(E190D/E391C)$_3\gamma$(R84C) were mixed in a molar ratio of 2:1 and incubated for $>$2 days in the presence of 200 mM NaCl and 100 mM DTT at 4 °C and pH 7.0. The chimera $\alpha_3\beta$(E190D)$_2\beta$(E391C)γ(R84C) was prepared by mixing solutions of $\alpha_3\beta$(E190D)$_3\gamma$(R84C) and $\alpha_3\beta$(E391C)$_3\gamma$(R84C) in a molar ratio of 2:1.

Rotation Assay. The rotary motion of $F_1^{\alpha\beta\gamma}$ was visualized by attaching a magnetic bead ($<$0.2 μm; Seradyn) onto the γ-subunit of $F_1^{\alpha\beta\gamma}$ and immobilizing the $\alpha_3\beta_3$ ring on a Ni-NTA-modified glass surface. Phase-contrast images of the rotating bead were obtained with an inverted optical microscope (IX-70; Olympus) equipped with magnetic tweezers (30). The image was captured with a CCD camera (FC300M; Takenaka) and recorded with a DV-CAM (DSR-11; Sony) at 30 fps. The recorded images were analyzed with image analysis software (Celery; Library) or a custom-made program (K. Adachi, Waseda University). The experimental procedures of the rotation assay for β-γ cross-linking were mostly the same as those reported (16), except for the content of the buffer. The basal buffer for the rotation assay contained 50 mM Hepes-KOH at pH 8.0, 50 mM KCl, 2 mM $MgCl_2$, 1 mM phospho(enol)pyrubate, 0.1 mg/ml pyrubate kinase, 5 mg/ml BSA, and 1 mM DTT. For β-γ cross-linking, 200 μM DTNB was added to the basal buffer, from which DTT and BSA were omitted. The rotation assay for AMP-PNP and/or NaN_3 inhibition was carried out in the buffer containing 50 mM Mops-KOH at pH 7.0, 50 mM KCl, 2 mM $MgCl_2$, 5 mg/ml BSA, and the indicated amount of nucleotides and NaN_3.

ACKNOWLEDGMENTS. We thank R. Hasegawa and Y. Iko-Tabata for technical assistance, W. Allison (University of California, San Diego) for plasmid vectors of mutant $TF_1^{\alpha\beta\gamma}$ from *Bacillus* PS3, M. Yoshida for discussion, and K. Adachi for the custom image analysis program. This work was partly supported by Grant-in-Aid for Scientific Research 18074005 (to H.N.) from the Ministry of Education, Culture, Sports, Science, and Technology of Japan.

1. Cross RL (2000) The rotary binding change mechanism of ATP synthases. *Biochim Biophys Acta* 1458:270–275.
2. Dimroth P, von Ballmoos C, Meier T (2006) Catalytic and mechanical cycles in F-ATP synthases: Fourth in the Cycles Review Series. *EMBO Rep* 7:276–282.
3. Senior AE (2007) ATP synthase: Motoring to the finish line. *Cell* 130:220–221.
4. Yoshida M, Muneyuki E, Hisabori T (2001) ATP synthase: A marvelous rotary engine of the cell. *Nat Rev Mol Cell Biol* 2:669–677.
5. Boyer PD (1997) The ATP synthase: A splendid molecular machine. *Annu Rev Biochem* 66:717–749.
6. Oster G, Wang H (2000) Reverse engineering a protein: The mechanochemistry of ATP synthase. *Biochim Biophys Acta* 1458:482–510.
7. Noji H, Yasuda R, Yoshida M, Kinosita K, Jr (1997) Direct observation of the rotation of F1-ATPase. *Nature* 386:299–302.
8. Diez M, *et al.* (2004) Proton-powered subunit rotation in single membrane-bound F0F1-ATP synthase. *Nat Struct Mol Biol* 11:135–141.
9. Tsunoda SP, Aggeler R, Yoshida M, Capaldi RA (2001) Rotation of the c-subunit oligomer in fully functional F1Fo ATP synthase. *Proc Natl Acad Sci USA* 98:898–902.
10. Abrahams JP, Leslie AG, Lutter R, Walker JE (1994) Structure at 2.8-Å resolution of F1-ATPase from bovine heart mitochondria. *Nature* 370:621–628.
11. Weber J, Senior AE (1997) Catalytic mechanism of F1-ATPase. *Biochim Biophys Acta* 1319:19–58.
12. Menz RI, Walker JE, Leslie AG (2001) Structure of bovine mitochondrial F(1)-ATPase with nucleotide bound to all three catalytic sites: Implications for the mechanism of rotary catalysis. *Cell* 106:331–341.
13. Yasuda R, Noji H, Yoshida M, Kinosita K, Jr, Itoh H (2001) Resolution of distinct rotational substeps by submillisecond kinetic analysis of F1-ATPase. *Nature* 410:898–904.
14. Shimabukuro K, *et al.* (2003) Catalysis and rotation of F1 motor: Cleavage of ATP at the catalytic site occurs in 1 ms before 40 degree substep rotation. *Proc Natl Acad Sci USA* 100:14731–14736.
15. Adachi K, *et al.* (2007) Coupling of rotation and catalysis in F(1)-ATPase revealed by single-molecule imaging and manipulation. *Cell* 130:309–321.
16. Watanabe R, Iino R, Shimabukuro K, Yoshida M, Noji H (2008) Temperature-sensitive reaction intermediate of F1-ATPase. *EMBO Rep* 9:84–90.
17. Yasuda R, *et al.* (2003) The ATP-waiting conformation of rotating F1-ATPase revealed by single-pair fluorescence resonance energy transfer. *Proc Natl Acad Sci USA* 100:9314–9318.
18. Bowler MW, Montgomery MG, Leslie AG, Walker JE (2006) How azide inhibits ATP hydrolysis by the F-ATPases. *Proc Natl Acad Sci USA* 103:8646–8649.
19. Bowler MW, Montgomery MG, Leslie AG, Walker JE (2007) Ground-state structure of F1-ATPase from bovine heart mitochondria at 1.9-Å resolution. *J Biol Chem* 282:14238–14242.
20. Hirono-Hara Y, *et al.* (2001) Pause and rotation of F(1)-ATPase during catalysis. *Proc Natl Acad Sci USA* 98:13649–13654.
21. Gao YQ, Yang W, Karplus M (2005) A structure-based model for the synthesis and hydrolysis of ATP by F1-ATPase. *Cell* 123:195–205.
22. Kagawa R, Montgomery MG, Braig K, Leslie AG, Walker JE (2004) The structure of bovine F1-ATPase inhibited by ADP and beryllium fluoride. *EMBO J* 23:2734–2744.
23. Koga N, Takada S (2006) Folding-based molecular simulations reveal mechanisms of the rotary motor F1-ATPase. *Proc Natl Acad Sci USA* 103:5367–5372.
24. Sun SX, Wang H, Oster G (2004) Asymmetry in the F1-ATPase and its implications for the rotational cycle. *Biophys J* 86:1373–1384.
25. Bandyopadhyay S, Allison WS (2004) The ionic track in the F1-ATPase from the thermophilic *Bacillus* PS3. *Biochemistry* 43:2533–2540.
26. Gibbons C, Montgomery MG, Leslie AG, Walker JE (2000) The structure of the central stalk in bovine F(1)-ATPase at 2.4-Å resolution. *Nat Struct Biol* 7:1055–1061.
27. Ma J, *et al.* (2002) A dynamic analysis of the rotation mechanism for conformational change in F(1)-ATPase. *Structure (London)* 10:921–931.
28. Rodgers AJ, Wilce MC (2000) Structure of the gamma-epsilon complex of ATP synthase. *Nat Struct Biol* 7:1051–1054.
29. Ariga T, Muneyuki E, Yoshida M (2007) F1-ATPase rotates by an asymmetric, sequential mechanism using all three catalytic subunits. *Nat Struct Mol Biol* 14:841–846.
30. Hirono-Hara Y, Ishizuka K, Kinosita K, Jr, Yoshida M, Noji H (2005) Activation of pausing F1 motor by external force. *Proc Natl Acad Sci USA* 102:4288–4293.
31. Dittrich M, Hayashi S, Schulten K (2004) ATP hydrolysis in the βTP and βDP catalytic sites of F1-ATPase. *Biophys J* 87:2954–2967.
32. Yang W, Gao YQ, Cui Q, Ma J, Karplus M (2003) The missing link between thermodynamics and structure in F1-ATPase. *Proc Natl Acad Sci USA* 100:874–879.
33. Kabaleeswaran V, Puri N, Walker JE, Leslie AG, Mueller DM (2006) Novel features of the rotary catalytic mechanism revealed in the structure of yeast F1 ATPase. *EMBO J* 25:5433–5442.
34. Braig K, Menz RI, Montgomery MG, Leslie AG, Walker JE (2000) Structure of bovine mitochondrial F(1)-ATPase inhibited by Mg^{2+} ADP and aluminium fluoride. *Structure (London)* 8:567–573.
35. Ahmad Z, Senior AE (2005) Identification of phosphate binding residues of *Escherichia coli* ATP synthase. *J Bionenerg Biomembr* 37:437–440.
36. Meiss E, Konno H, Groth G, Hisabori T (2008) Molecular processes of inhibition and stimulation of ATP synthase caused by the phytotoxin tentoxin. *J Biol Chem* 283:24594–24599.
37. Rondelez Y, *et al.* (2005) Highly coupled ATP synthesis by F1-ATPase single molecules. *Nature* 433:773–777.

Supporting Information

Okuno *et al.* 10.1073/pnas.0805828106

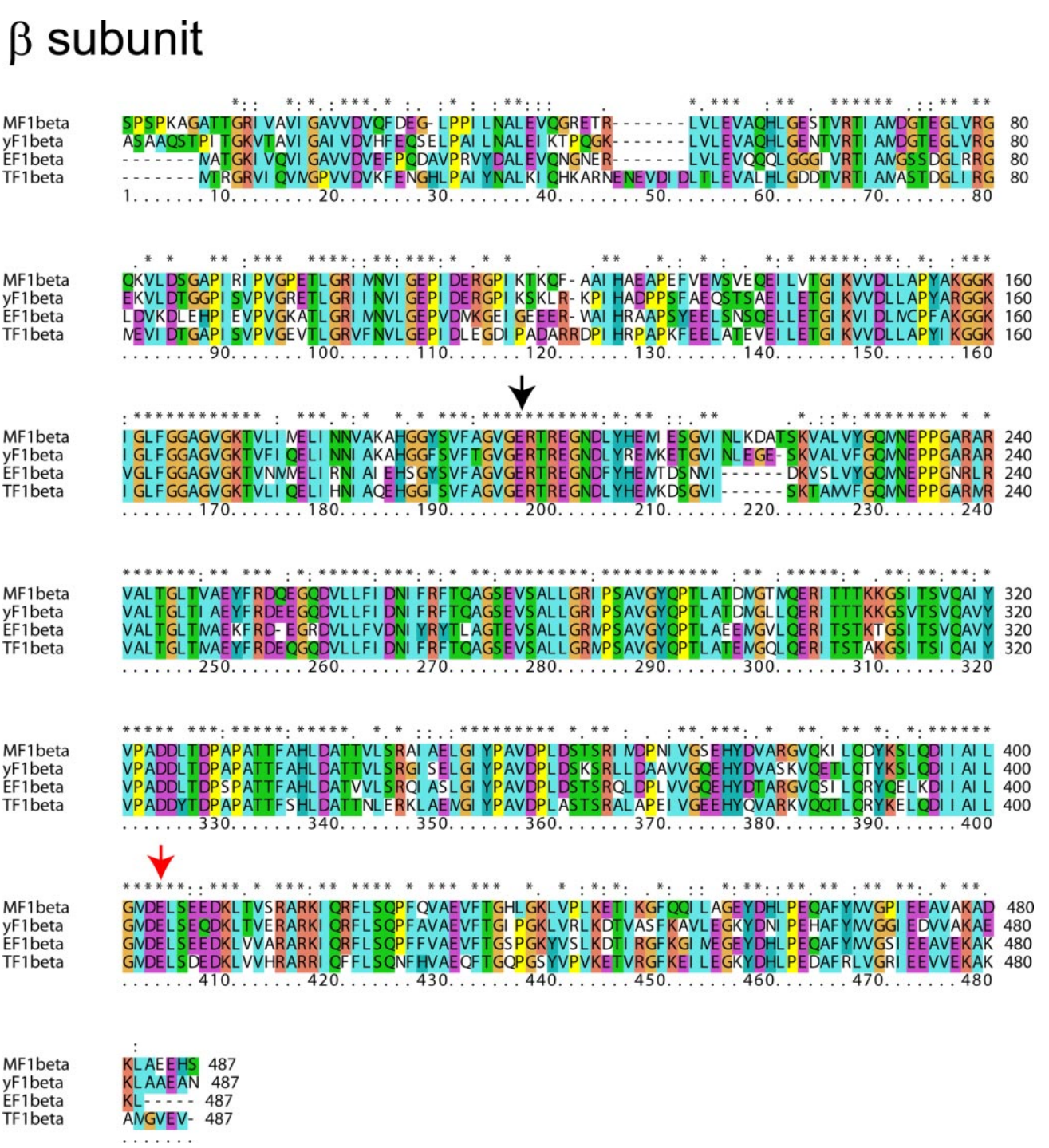

Fig. S1. Sequence alignment of the β-subunit of F_1 from bovine mitochondoria (MF_1), yeast mitochondoria (yF_1), *Escherichia coli* (EF_1), and thermophilic *Bacillus* PS3 (TF_1). A red arrow indicates the position of mutation into cysteine for cross-link. A black arrow indicates the mutated position of the βE190D. Sequence alignment was carried out by using ClustalX 2.0.9 software (1). Amino acid residues of precursor peptides were not included for alignment.

1. Larkin MA, *et al.* (2007) *Bioinformatics* 23:2947–2948.

γ subunit

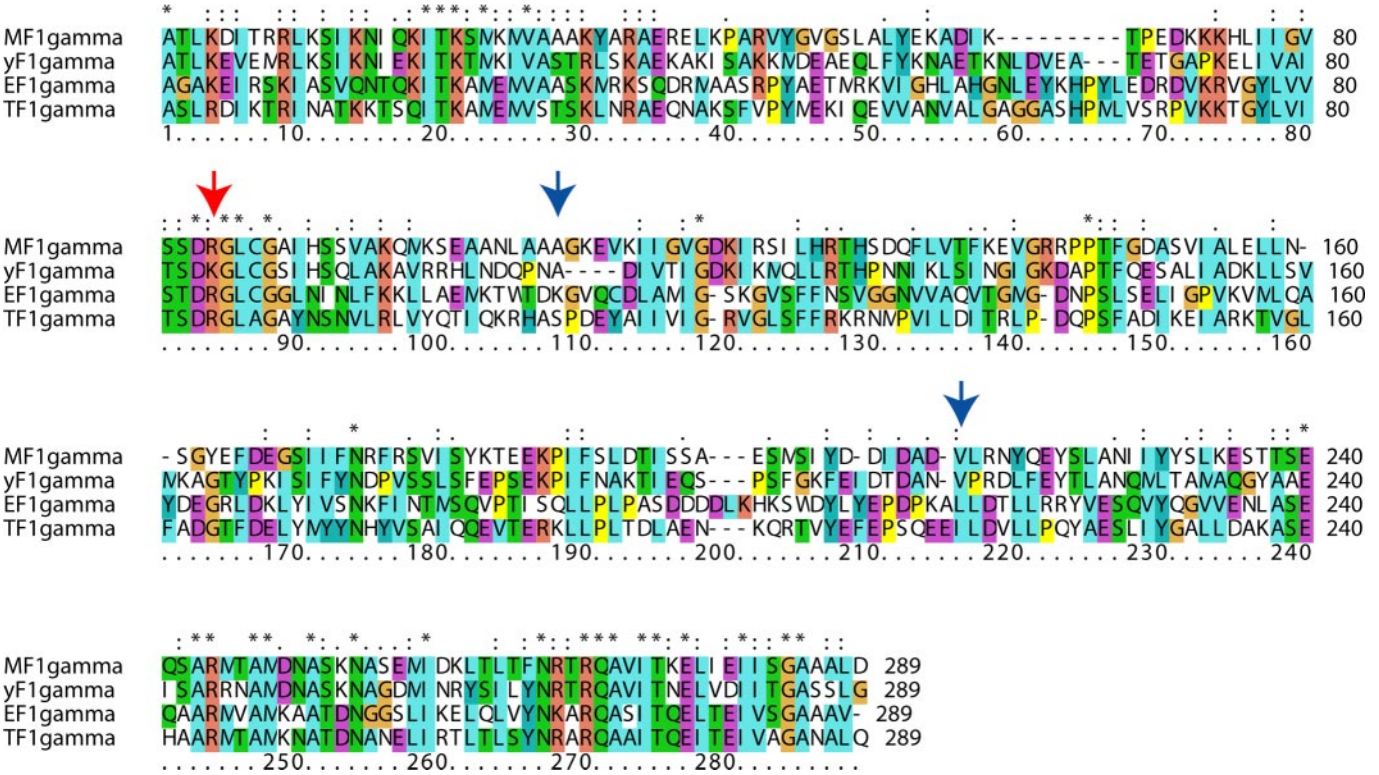

Fig. S2. Sequence alignment of the γ-subunit of MF_1, yF_1, EF_1, and TF_1. A red arrow indicates the position of mutation into cysteine for cross-link. Blue arrows indicate the mutated positions to cysteine for biotinylation. Sequence alignment was carried out by using ClustalX 2.0.9 software (1).

1. Larkin MA, *et al.* (2007) *Bioinformatics* 23:2947–2948.

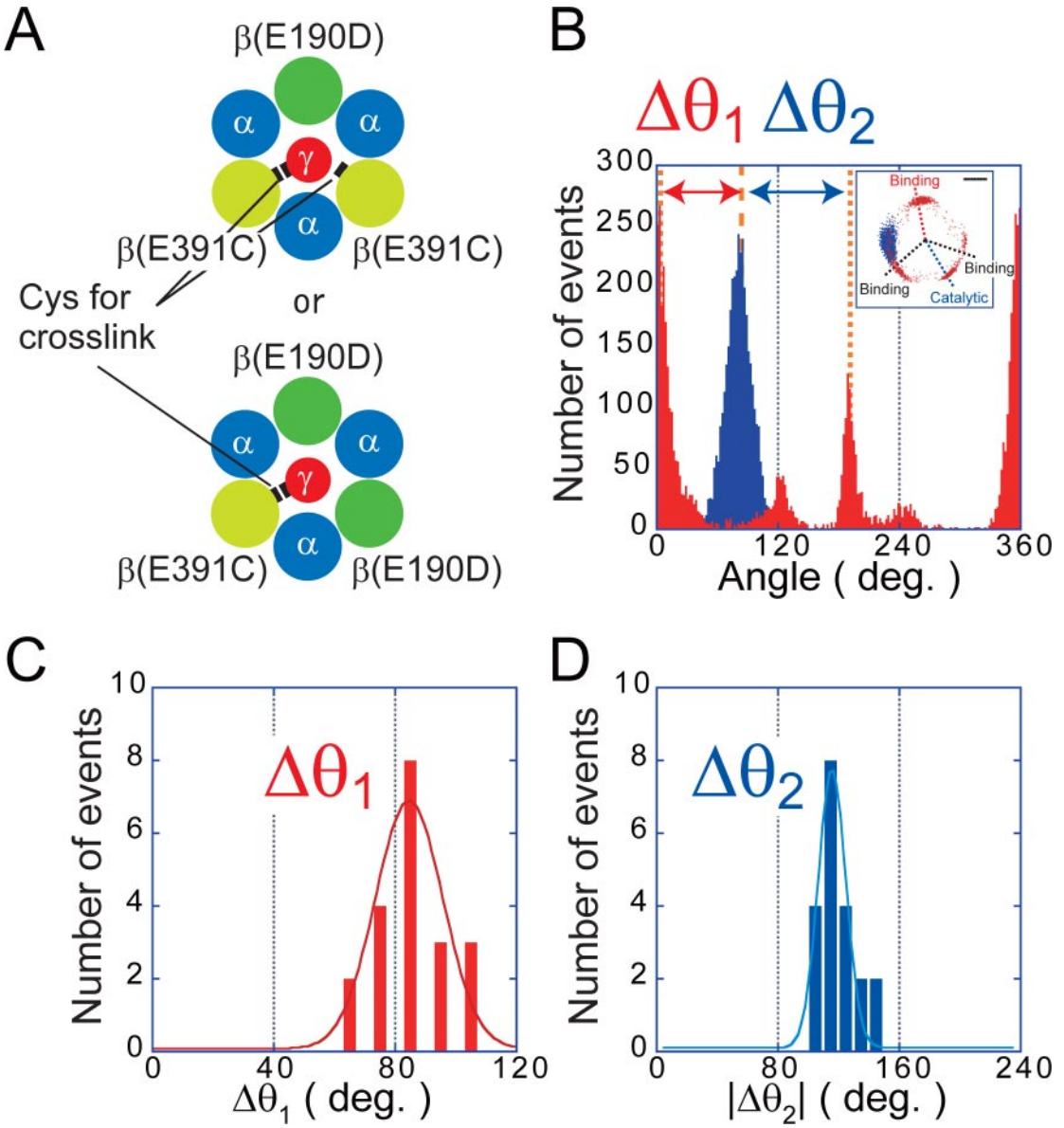

Fig. S3. The pausing positions of chimera $F_1^{\alpha\beta\gamma}$, $\alpha_3\beta$(E190D)$_2\beta$(E391C)γ(R84C) or $\alpha_3\beta$(E190D)β(E391C)$_2\gamma$(R84C). (*A*) Schematic images of the chimera $F_1^{\alpha\beta\gamma}$ molecules. (*B*) Typical angle distribution of a $\alpha_3\beta$(E190D)β(E391C)$_2\gamma$(R84C) molecule. Red bars represent the angular position of free rotation before cross-link. Blue bars represent pausing angular position after cross-link. (*Inset*) The trace of centroid of the bead image. (Scale bar: 100 nm.) (*C*) Histogram of angle deviation of pausing position from the nearest binding dwell angle on the clockwise side ($\Delta\theta_1$). (*D*) Histogram of angle deviation of pause position from the catalytic angle of βE190D. Because $\alpha_3\beta$(E190D)β(E391C)$_2\gamma$(R84C) paused at two catalytic angles that correspond to those of wild-type β-subunits, in other words at the position about $\pm$120° from the catalytic angle of βE190D, distribution of absolute values is given. In *C* and *D*, data from two kind of chimera were combined. The total molecule and trial numbers were 11 [of them, two were $\alpha_3\beta$(E190D)$_2\beta$(E391C)γ(R84C)] and 20, respectively.